Star-shaped Triphenylene-triazine Multi-stimuli Responsive Discotic Liquid Crystals: Synthesis, Properties and Applications

Zeng Chongyang, Hu Ping, Wang Biqin, Fang Wenyan, Zhao Keqing, Donnio Bertrand, Bertrand Donnio

Star-shaped triphenylene-triazine multi-stimuli responsive discotic liquid crystals: synthesis, properties and applications

Chong-Yang Zeng [a], Ping Hu [a], Bi-Qin Wang [a], Wen-Yan Fang [b], Ke-Qing Zhao *[,a], Bertrand Donnio [c]

[a] College of Chemistry and Materials Science, Sichuan Normal University, Chengdu, China.

[b] School of Chemistry and Materials Engineering, Huainan Normal University, Anhui Huainan, China.

[c] Institut de Physique et Chimie des Matériaux de Strasbourg (IPCMS), CNRS-Universite de Strasbourg (UMR 7504), Strasbourg 67034, Cedex 2, France.

Acta Chimica Sinica. **2023**, *81*, 469-479. DOI: 10.6023/A23010006

* E-mail: kqzhao@sicnu.edu.cn

Received : January 10, 2023; Published : April 14, 2023

Project supported by the National Natural Science Foundation of China (Nos. 51773140, 51973143). 国家自然科学基金(Nos. 51773140, 51973143)资助.

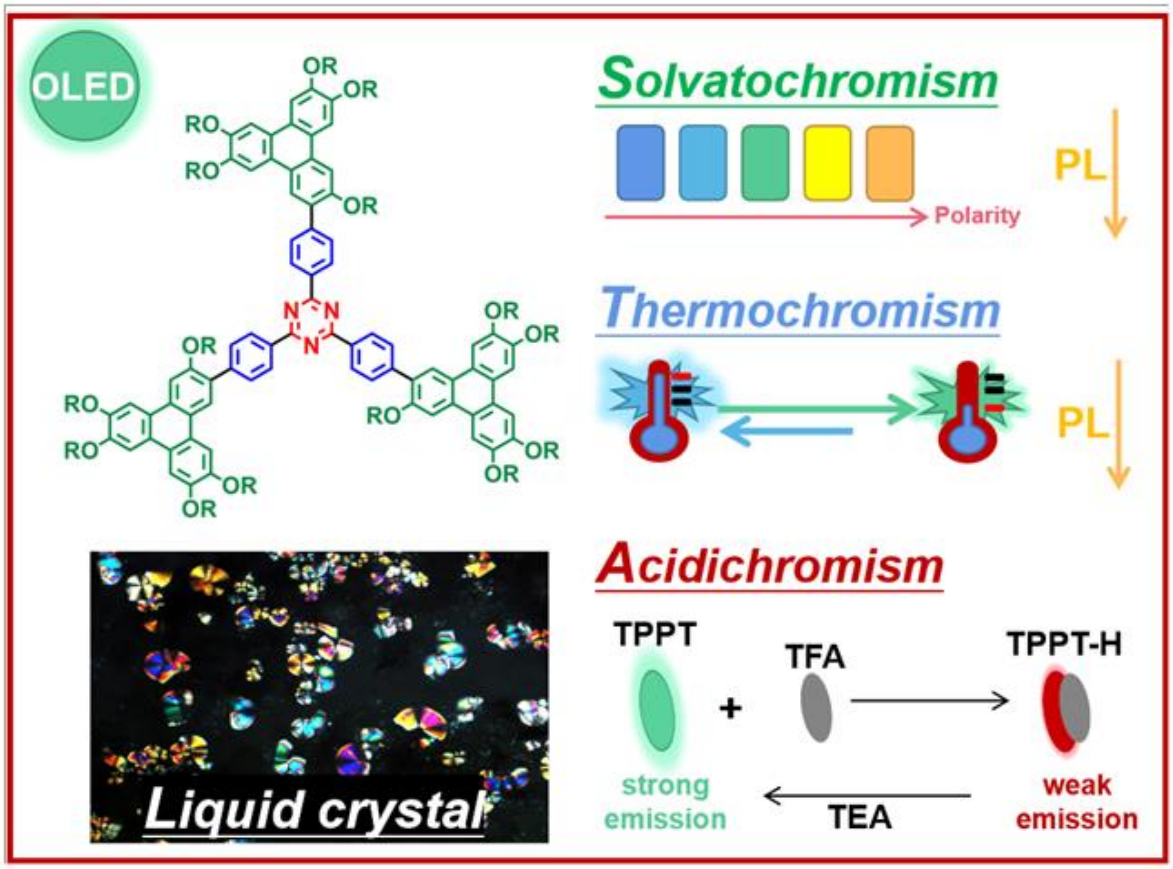

Abstract Electronic and optical properties of π-conjugated materials are determined by their molecular structures and their supramolecular architectures. Discotic liquid crystals consist of π-conjugated aromatic cores surrounded by various connected peripheral alkyl chains, which then self-organize into two-dimensional discotic columnar mesophases. They are of particular interest as they can be applied as charge carrier transport channels for optical and electronic thin-film devices. Order and dynamics are two unique features of discotic liquid crystalline semiconductors. Three star-shaped phenylene-bridged 1,3,5-triazine-triphenylene discotic liquid crystals **TPPT***n* (*n* = 6, 8, 12) were synthesized by Suzuki-Miyaura cross-coupling reaction and characterized by ^{1}H and ^{13}C NMR, HRMS and EA. These **TPPT***n* show good thermal stability by thermogravimetric analysis (TGA), with decomposition temperatures higher than 350 °C. UV-vis absorption and fluorescence measurements show that they possess outstanding fluorescence emission in solution, thin films and in solid state, and that the length of the alkoxy chains affects the fluorescence properties in films or solid state, due to slight changes of the molecular aggregation. **TPPT***n* display aggregation-induced emission (AIE): the longer the alkoxy chains, the stronger the AIE; here, AIE effectively overcomes the disadvantage of aggregation caused quenching (ACQ) of π-extended discotic liquid crystalline molecules. Further, **TPPT**6 exhibits a significant solvatochromism from blue to orange with increasing solvent polarity, due to intramolecular charge transfer (ICT), which thus provides a possibility for visual recognition of the solvent polarity. The fluorescence absolute quantum yield is up to 43%. Moreover, **TPPT**6 exhibits enhanced temperature-responsive fluorescence with increasing temperature in solution, which is different from the temperature quenching observed for traditional molecules; moreover, the fluorescence exhibits a reversible switching from green to blue with the increase/decrease of the temperature. Furthermore, **TPPT**6 has a clear acid-base stimulus-responsive fluorescence in the presence of CF_3COOH/Et_3N. ^{1}H NMR titration proves that the protonation of the triazine core is the main mechanism to acid discoloration. Based on the acid-base stimuli response phenomena, two kinds of fluorescent safety inks have been designed and demonstrated. DSC, POM and S/WAXS indicate that these star-shaped molecules **TPPT***n* have liquid crystal properties, self-organizing into columnar rectangular (Col_{rec}) mesophase over large temperature range as wide as 278 °C. Trifluoroacetic acid (CF_3COOH) modulates successfully the mesomorphic behavior of **TPPT***n* by ionization of the triazine core. Finally, **TPPT**6 also displays electroluminescent properties, which can be used for the preparation of security inks and has been applied to green organic light-emitting diode (OLED), for which the luminous efficiency of the OLED reaches 7.41 lm/W. In conclusion, the star-shaped triphenylene-triazine **TPPT***n* feature many potential applications as liquid crystalline semiconductors, fluorescent sensing, information encryption and organic light-emitting diodes.

Keywords Triphenylene, triazine, multi-stimuli response, discotic liquid crystals, AIE, Suzuki cross-coupling reaction.

1 Introduction

Just as a chameleon changes colour in response to its external environment, so too do smart synthesized stimulus-responsive luminescent materials (SRLMs) have the ability to respond to various changes in their external environment (light, electricity, heat, force, acid, concentration, etc.) [1]. SRLMs have potential applications in fluorescence anti-counterfeiting [2], chemical detection/sensing [3, 4], cell imaging [5], light-emitting diodes (LEDs) [6], etc. Particularly in the context of the new coronavirus epidemic, their development and design in the biomedical field have been strongly encouraged by researchers [7, 8]. In such a context, heteroatomic polycyclic aromatic sub-units [9, 10] have been widely used in the design of new stimuli-responsive molecules due to specific electronic properties and coordination ability of the heteroatoms. Among the many conjugated heteroatomic molecular units available, the cyclic 1,3,5-homotriazine structure is particularly well suited, as it enables the conjugated system to be easily extended to obtain luminescent properties. Combined with the strong electronegativity of the N atoms, which determines their excellent electron accepting ability, these two features are attractive for the construction of intramolecular charge-transfer donor-acceptor (D-A) molecules that also offer fluorescence versatility [11]. The nitrogen lone electron pair of the triazine ring is also a good hydrogen-bond acceptor and a quaternizable unit, facilitating the construction of various reactive systems based on ion, acid-base and metal-ligand stimuli [12,13]. In summary, 1,3,5-triazine is an excellent unit for the construction of multi-stimuli responsive fluorescent materials. However, although the study of triazine derivatives has received some attention in the fields of optics (e.g., two-photon absorption [14], OLEDs [15], etc.), pharmacology [16] and supramolecular materials [17], reports on luminescent liquid-crystal semiconductor materials responsive to multiple stimuli are few.

In addition to the luminescent properties, the unique star shape of 1,3,5- homotriazine can be used as a module for the design of macromolecular liquid crystal materials [18]. However, due to their twisted propeller structure, it is often difficult for these molecules to exhibit high-order columnar stacking. Common strategies to overcome this drawback include lengthening the flexible chains to obtain nematic liquid crystals [19,20], increasing the number of flexible chains and extending the π-conjugated system [21-24], stabilising the twisted triazine ring while reducing the rotational degree of freedom with the help of hydrogen bonding, and microphase separation of fluoroalkyl chains to obtain stable hexagonal columnar phases [25-29]. Discotic liquid crystals [33-35], with the representative triphenylene [30-32], have been widely investigated in the field of organic semiconductor materials and displays because of their highly ordered self-assembled intermediate phases. The formation of liquid-crystalline phases is facilitated by the linking of triazine units to triphenylene structures via flexible chains [36-39]. This study focuses on the stimulus-responsive self-assembled liquid crystalline, optical and luminescence properties of novel triphenylene-triazine derivatives, both for their academic value and for their application potential.

Typically, discotic liquid crystals exhibit strong fluorescence in dilute solution due to the flatness of the aromatic core, while in the aggregated state, the strong intermolecular π-πstacking consumes the energy absorbed by the stack and exhibits aggregation-caused fluorescence quenching (ACQ) [40,41]. Liquid crystal displays do not emit light directly, and the need to supplement additional light sources leads to increase the energy consumption, limiting the application of liquid crystal materials. The discovery of aggregation-induced luminescence (AIE) and the proposed

mechanism makes it possible to effectively overcome the ACQ effect, which has been difficult to avoid for a long time [42,43]. In this respect, distorted molecules [44,45] can produce strong fluorescence emission by aggregation. Therefore, the design and synthesis of AIE discotic liquid crystals are very valuable [46], since such materials can be applied to light-emitting diode OLEDs [47]. Triphenylene derivatives have been reported as red and blue OLED materials (mainly blue light) [48-52], whilst green triphenylene materials are rare and have high turn-on voltage and low luminous efficacy [48,51].

In this manuscript, a series of mesomorphous D-A **TPPT***n* compounds were simply and efficiently synthesised by Pd-catalyzed Suzuki-Miyaura cross-coupling reaction between 1,3,5-homotriazine as the electron-acceptor stimuli-responsive luminescent unit and triphenylene as the electron-donor liquid-crystalline matrix. The molecular design was based on the rigid linkage triphenylene-triphenyltriazine to obtain star compounds (see Route 1). This study focusses on the stimulus-responsive fluorescence and self-assembled mesomorphous properties of **TPPT***n*, as well as exploring possible new applications in acid-base sensing, information encryption and OLED devices.

2 Results and Discussion

Based on the experience of our group in the design and synthesis of discotic liquid crystal molecules [53,54], three target compounds, **TPPT**6/8/12, were synthesised simply and efficiently by Suzuki-Miyaura cross-coupling between bromotriphenylene and triazine phenylboronic acid derivatives. The detailed synthetic methods of the intermediates and the target compounds are shown in the Appendix. Their complete characterization was carried out by nuclear magnetic resonance (^{1}H and ^{13}C NMR) and high-performance liquid chromatography (HPLC). High resolution mass spectrometry (HRMS) and elemental analysis (EA) were used to characterise the target compounds (Figures S1-S12).

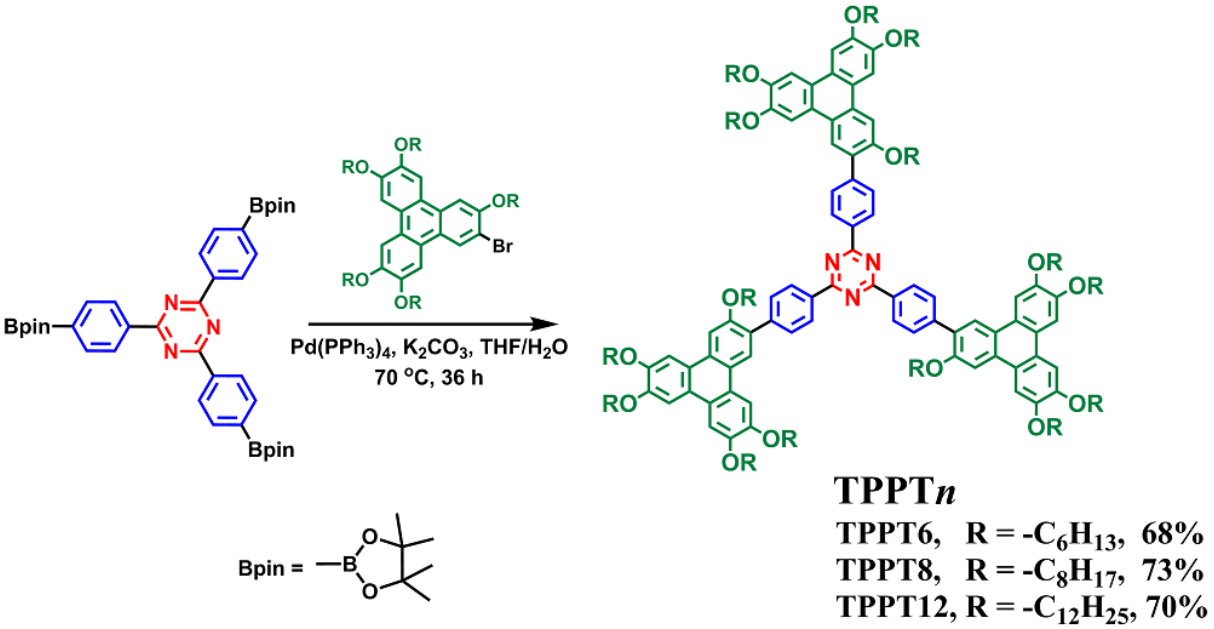

Scheme 1. Star-shaped compounds triphenylene-phenyl-triazine **TPPT***n*: molecular structure, nomenclature, synthesis and yields.

2.1 Thermal stability

Thermal stability is a crucial parameter for organic functional materials used in devices. Therefore, thermogravimetric analysis (TGA) of **TPPT**6/8/12 was first carried out under N_2 atmosphere with a heating rate of 10 °C/min, and the results are shown in Figure S13 and Table S1. The onsets of the thermal decomposition (at 5% weight loss) were found at 375, 364 and 355 °C, respectively, which indicates a very high thermal stability for **TPPT***n* compounds.

2.2 Photophysical properties and solvatochromism

Optical properties of the **TPPT***n* were investigated in tetrahydrofuran (THF) solution and in solid and thin film (Figure 1). The two main absorption peaks of **TPPT**6/8/12 in THF solution are located at 278 and 364 nm, and the molar extinction coefficients of both peaks are greater than 10^4 L cm^{-1}-mol^{-1}, which proves that there is intramolecular electron transition, and that the change of alkyl-chain length only causes a small change of the absorbance intensity. Fluorescence measurements of **TPPT**6/8/12 in solution, thin film and solid state (Figures 1b and S15) show good emission properties, and indicate a bimodal luminescence property in solution and solid state.

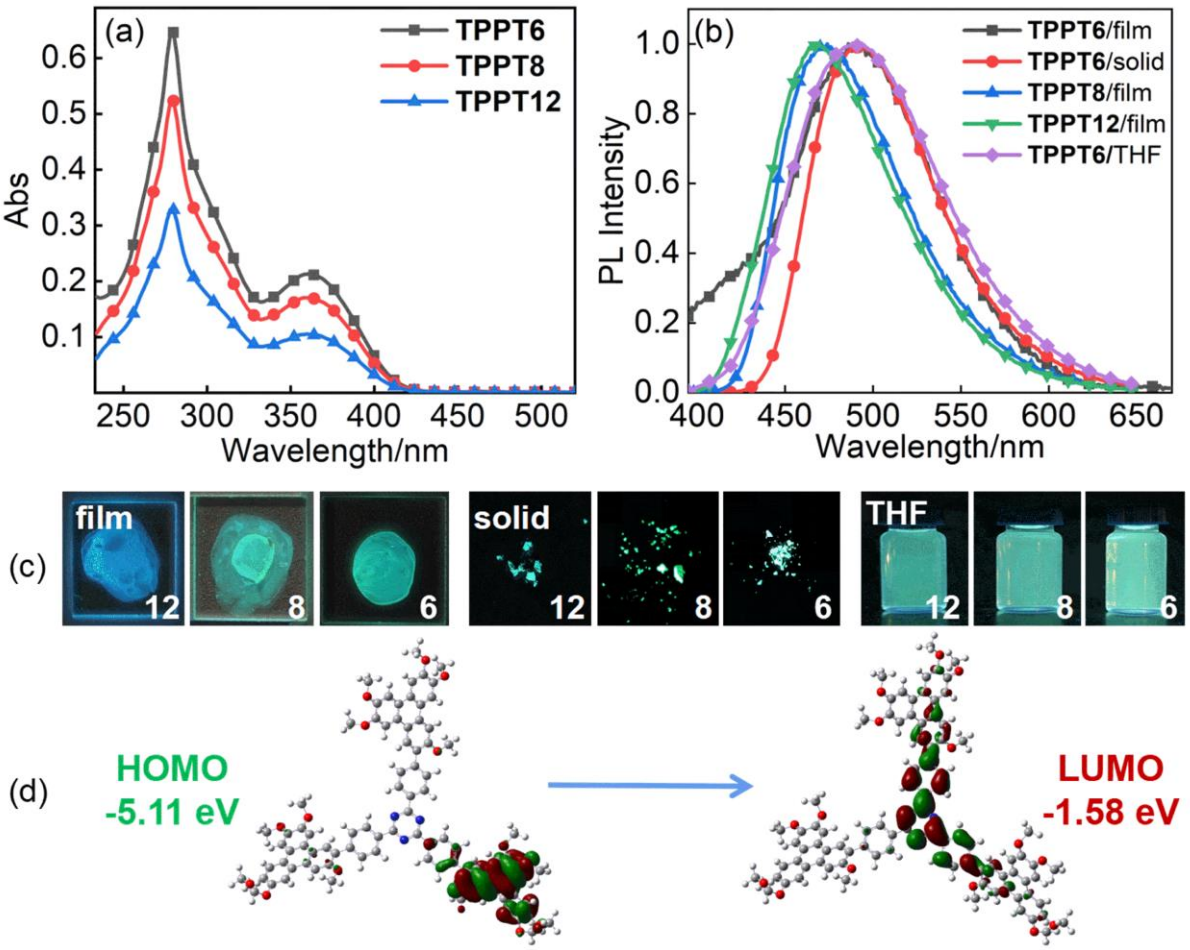

Figure 1. UV-Vis absorption spectra of **TPPT**6/8/12 in THF (a); fluorescent emission spectra (b); fluorescence photos of **TPPT***n* in various states (c); electron distribution in frontier molecular orbitals of **TPPT**1 (d).

The emission of **TPPT**6/8/12 is almost unchanged in solution for the three compounds, but the emission wavelength shows a certain degree of blueshift with the increase of

the alkoxyl chain in both solid and thin film states, which evidences the influence of the aliphatic chain on the molecular aggregation state [55] as later confirmed by small-angle X-ray scattering (see below, SAXS, Figure S28).

Since absorption and emission spectra of the three terms of the **TPPT***n* series in solution are not very different, the subsequent photophysical property studies were carried out on **TPPT**6 only. The geometrically optimized configurations of the **TPPT**1 molecule and the electronic density distributions of the ground and excited states were investigated at the level of theory of B3LYP/6-31G (d) by using density-functional theory (DFT). The results are shown in Figures 1d, S19 and S20. The optimal configuration of **TPPT**1 molecule is a twisted propeller-like molecule, and from the frontier molecular orbital (FMO) energy levels, it is clear that **TPPT** molecule is a typical D-A molecule.

For the HOMO, the electron density is mainly distributed on the electron donor triphenylene unit with high electron cloud density, while for the LUMO, the electron density distribution is significantly shifted due to the strong electron absorption of the electron acceptor triazine ring, which is mainly distributed on the central triazine ring and its attached phenyl groups, with the participation of triphenylene. It can be seen that **TPPT** molecule has an obvious ground state - excited state intramolecular charge transfer (ICT), which is the main reason why **TPPT** molecule has a strong electron-withdrawing ability, which affects the fluorescence emission of **TPPT** molecule.

In order to investigate the effect of the solvent polarity on the photophysical properties of **TPPT**6, UV-visible absorption and fluorescence emission were measured in six solvents, including cyclohexane (CHX), toluene and ethyl acetate (EA). The results are summarised in Figure 2, and Tables 1 Table S2 (see Supporting Information). The absorption band near 365 nm was slightly red-shifted with the increase of solvent polarity, and the fluorescence emission wavelength was red-shifted by 70 nm. The fluorescence intensity gradually decreases, and the fluorescence colour changes from blue to green and finally to dark orange-yellow.

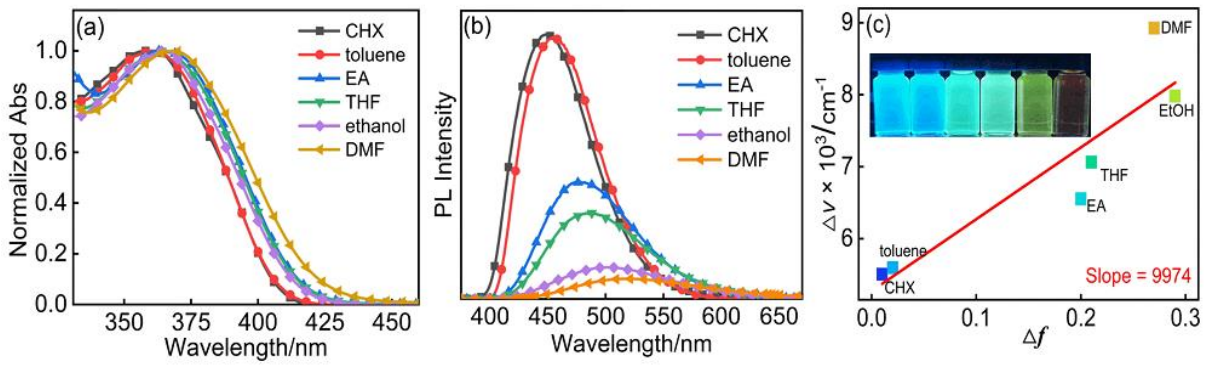

Figure 2. UV-Vis absorption spectra (a); fluorescence emission spectra (b) and Lippert-Mataga curve (c) of **TPPT**6 in different solvents, and inserted image is fluorescence photos (polarity increases from left to right).

The Lippert-Mataga curve (see Appendix 8 for the formula) shows a straight line with an upward slope (slope = 9947). This indicates that the dipole moment of the excited state is larger than that of the ground state (i.e., the polarity of the excited state is larger than that of the ground state) [56]. Therefore, the greater the solvent polarity, the greater the difference between the dipole moment of the excited state and the dipole moment of the ground state. i.e. the more polar excited state is stabilized in the more

polar solvent, the HOMO-LUMO energy gaps are reduced, and the luminescence wavelength is redshifted. At the same time, in a polar solvent, the dipole-dipole interaction in the solution increases, and the non-radiative decay is strengthened, the radiative channels are weakened or even closed, resulting in a decrease in fluorescence intensity [57]. The results show that **TPPT**6 has a strong solvatochromic behaviour and is the most important in the more polar solvents. This provides conditions for the visual recognition of solvent polarity, and **TPPT**6 has also been developed as a solvatochromic fluorescent light probe [58].

Table 1. Photophysical property parameters of **TPPT**6

Compound	Solvent	λ_a	ε (×10⁴)	λ_e	QY	$\Delta\nu$
TPPT6	CHX	360	19.62	449	43.02	5506
	toluene	362	21.27	454	42.20	5597
	EA	364	9.41	478	22.02	6552
	THF	364	24.89	490	18.44	7064
	EtOH	367	21.31	519	9.59	7980
	DMF	368	22.16	548	0.96	8925

[λ_a] longueur d'onde d'absorption UV (nm); [ε] coefficient d'absorption molaire (L mol^{-1} cm^{-1}); [λ_e] longueur d'onde d'émission (nm); [QY] rendement quantique de fluorescence (%); [Δν] valeur du décalage de Stokes (cm^{-1}).

2.3 Aggregation induction effect

As seen above, **TPPT**6 is soluble in most organic solvents, but not in H_2O. Therefore, the aggregation-inducing effect of **TPPT**6 was investigated using a mixture of tetrahydrofuran (THF) and H_2O, and the results are shown in Figure 3.

The UV absorption spectra (Figure 3a) shows that the absorption wavelength is redshifted and the band broadened with increasing water content. 3a). This is the result of the increase of effective π–conjugation due to the intermolecular accumulation of molecular aggregates, the higher the water content, the aggregation degree increases.

Variable concentration NMR (see Supporting Information, Figure S21) reveals that the chemical shifts of the hydrogen atoms of the aromatic nuclei shift to higher fields as the solution concentration increases. This is the result of the increased of intermolecular face-to-face π-π interactions between the molecules and the shielding of aromatic hydrogen atoms by the aromatic ring electron flow, which proves the existence of molecular aggregation phenomenon with increasing concentration [58-59]. Fluorescence spectra in pure THF shows that the fluorescence emission wavelength of **TPPT**6 is at 490 nm i.e. with lime green fluorescence. At 10% water content (v/v), the fluorescence intensity is halved and the emission wavelength is red-shifted to 515 nm with yellow-green fluorescence. This is because water is a polar solvent, the degree of molecular aggregation is very small at this time, and it is mainly affected by the solvation of the polar solvent. The energy absorbed by the shift is consumed by the dipole-dipole interaction between the polar solvents and the free torsion of covalent single bonds. The fluorescence intensity increases from 10% to 90% of water content, and the solution with 90% of water content shows a bright greenish fluorescence, an unbiguous proof of the AIE effect. This is because **TPPT**6 is a three-bladed propeller twisted molecule. During water content increase, the

molecular aggregation gradually blocks intramolecular rotations, suppressing the non-radiative decay. The non-radiative decay then is inhibited, the radiative channel is strengthened, and the energy of the excited state is released in the form of radiation, resulting in strong fluorescence [41-43]. It is noteworthy that a fluorescence burst occurrs at 10% water content, and the fluorescence spectra measured with a narrowing gradient in the interval of less than 10% water content (Figure 3d). The R2 = 0.986, indicates that **TPPT**6 has the potential to be used in the detection of micro-amounts of water.

In addition, the comparison of the AIE fluorescence spectra of **TPPT**6/8/12 (see Supporting Information, Figure S16) reveals that the alkyl chain-length has a significant effect on the AIE phenomenom, with a fluorescence enhancement of 1.8-fold for **TPPT**8 and 2.5-fold for **TPPT**12, which is attributed to the increase of the hydrophobicity of the **TPPT** molecules, as well as the free twisting of the single molecule state, resulting in relatively stronger aggregation and more pronounced fluorescence in high water content solutions [55].

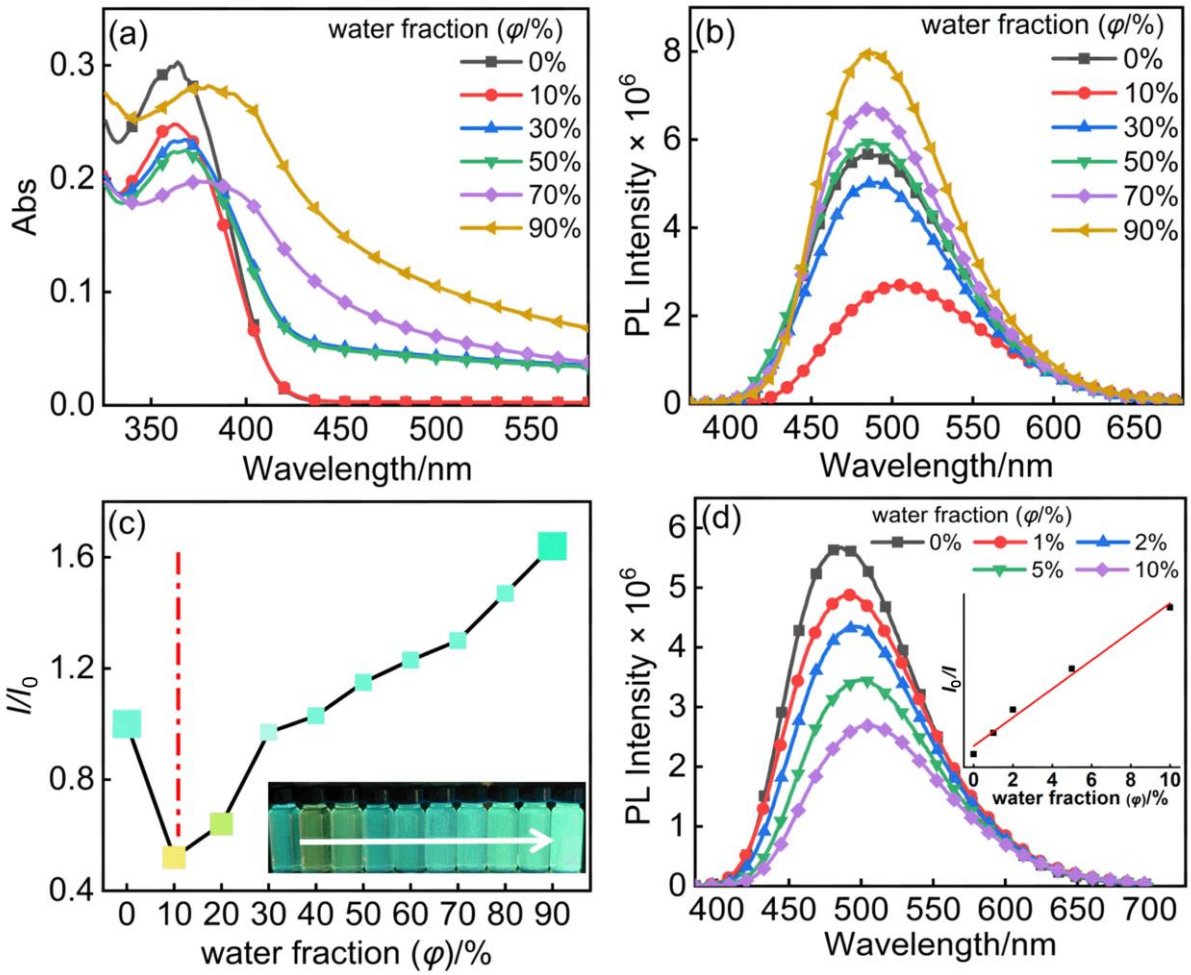

Figure 3. UV-Vis absorption spectra (a), PL emission spectra (b) and fluorescence intensity change map (c) of **TPPT**6 in THF/H_2O with different water fraction. (d) for the water fraction between 0～10% of the fluorescence spectra, inserted picture for the fluorescence quenching fitting curve.

2.4 Temperature stimulus response (thermochromic)

The thermochromic behaviour of **TPPT**6 in solution was investigated by UV-Vis absorption and fluorescence emission spectroscopy, and the results are shown in Figure 4. From room temperature to 75 °C, the absorption wavelength of **TPPT**6 in ethyl acetate solution shows a slight blueshifted trend. The fluorescence emission wavelength is blueshifted, from cyan to indigo blue. The change as the result of volatilisation of the solvent by heating i.e. change in concentration of the solvent, was ruled out by means of an immunity test (see Supporting Information, Figure S17).

Subsequent alternating cooling/heating cycles of the solution resulted in a reversible change in the emission wavelength (Figure 4b), demonstrating that this temperature-stimulated response change was not caused by the volatilisation of the solvent. The absence of significant changes in the UV spectra also demonstrated that the structure of the compound was not changed during the heating/cooling process. While conventional thermochromic molecules tend to show fluorescence burst at elevated temperatures, in contrast to **TPPT**6. It is hypothesised that this phenomenon may have arisen because the elevated temperature resulted in the decrease in the polarity of the solvent, the solvatation effect of the more polar solvents being weakened.

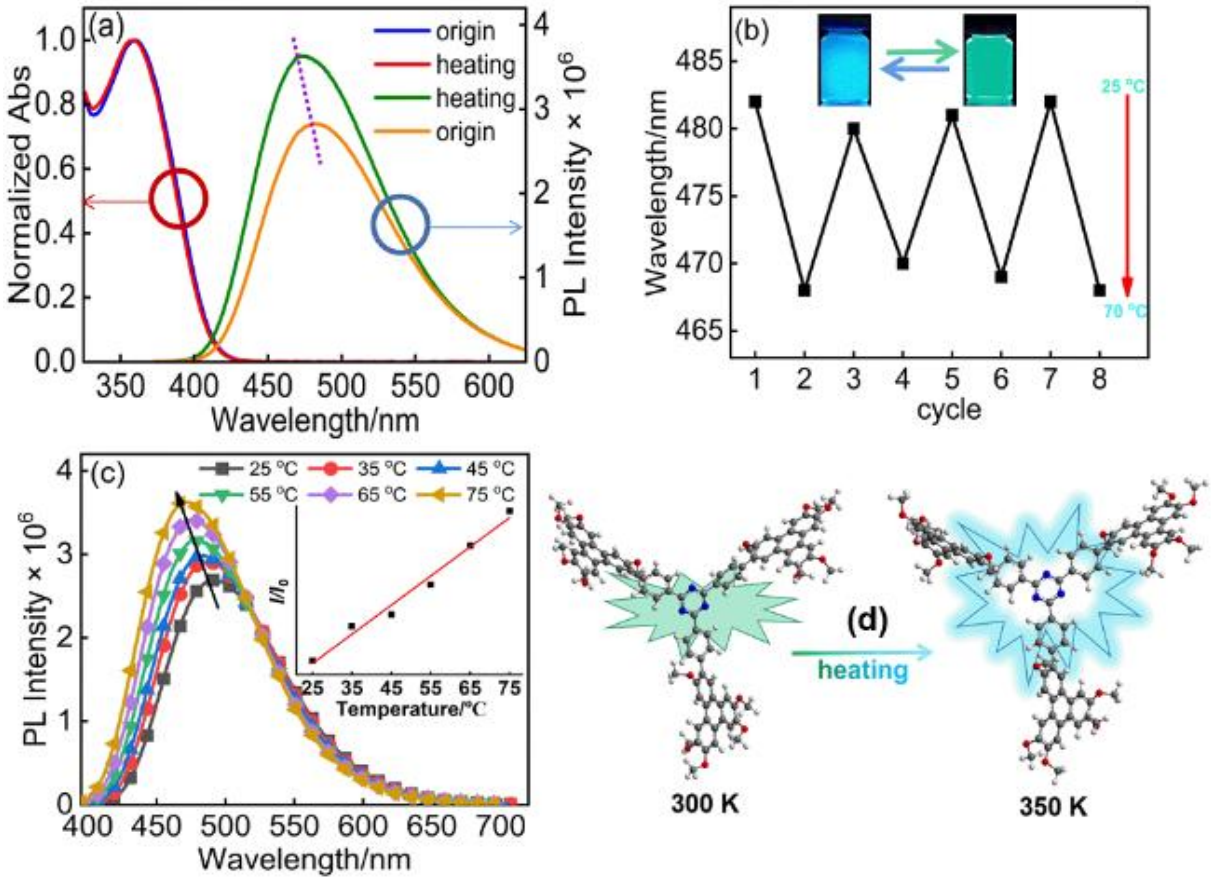

Figure 4. UV-Vis absorption and fluorescence spectra of **TPPT**6 in lower and higher temperature in CH_3COOEt (a); fluorescence wavelength variation with alternating heating-cooling (b); fluorescence spectra at 25~75 °C (c), insert, picture for the linear fitting of temperature and I/I_0; (d) the **TPPT** molecular conformations at 300 K and 350 K.

The increase in temperature also increases the hydrophobicity of the solvent, thus facilitating the transition of the **TPPT**6 molecules from distorted to planar molecules. The conformations of **TPPT** molecules at 300 K and 350 K were calculated by MMPF94 force field separately (Figure 4d). The conformation at 350 K is more planar. The π-bridge (phenyl) connecting the electron donor and the acceptor parts shows obvious planarisation, which is conducive to intramolecular charge transfer and fluorescence emission, and thus fluorescence enhancement. This phenomenon is consistent with the thermochromic behaviour of triphenylamine D-A derivatives in solution reported in the literature [60]. In addition, the face-to-face stacking between the target molecules in dilute solution is strong during cooling, and the energy transfer between the excited high-energy and the low-energy ground states consumes energy, whereas heating increases the intermolecular gap and decreases the intermolecular interactions leading to the fluorescence enhancement. The linear relationship between fluorescence intensity and temperature was observed in the range of 25-75 °C (R2 = 0.98). **TPPT**6 also shows similar temperature stimulation responses in trichloromethane, THF, and other solvents. Therefore, **TPPT**6 has potential applications in temperature sensors and thermometers.

2.5 Acid-base stimulus response (acid-induced discolouration)

The nitrogen atom in the triazine ring of the **TPPT**6 molecule has a lone pair of electrons that acts as a Lewis base accepting protons for protonation. Based on this, the effects of **TPPT**6 in chloroform were investigated in trifluoroacetic acid (TFA) and triethylamine (TEA) to study the acid/base stimulation response, and the results are shown in Figure 5.

UV shows that the absorption at 360 nm is weakened upon addition of TFA, and a new broad absorption band appears at 430 nm, with an obvious red shift, indicating that TFA interacts with **TPPT**6 to form a new ionic compound. The fluorescence is quenched after the addition of TFA, and the colour of the solution changes from light yellow to dark red in the visible, and green in UV light, and the quantum yield decreases from 22% to almost 0.

Subsequently Et_3N/CF_3COOH was added to the solution alternately, and the fluorescence changes reversibly. What is interesting here is that this reversible discolouration behaviour does not only occur in solution, but also in solid and thin film states (Figures 5e, 5f). A concentrated chloroform solution of **TPPT**6 was dropped onto filter paper or quartz glass, which dried naturally and showed a yellow colour and a strong greenish fluorescence under UV light. The filter paper was fumigated with TFA vapour, and the filter paper/film gradually turned orange-red, and the UV light showed a strong greenish fluorescence. The red colour faded and the fluorescence was restored by fumigation with TEA vapour. The fluorescence spectrum (Figure 5d) shows that the emission peak at 450 nm is greatly reduced after TFA fumigation and a new weak emission peak appears around 620 nm. This reversible change by acid/alkaline gas stimulation is attributed to the acid-base stimulus response. Experimental findings with **TPPT**6 showed the same discolouration phenomenon with HBr, TFA and trifluoromethanesulfonic acid (see Supporting Information, Figure S25).

The addition of TFA to the deuterated solution caused a high field shift of most of the aryl hydrogens (^{1}H NMR titration experiments, see Supporting Information, Figures S22-S24), suggesting a chemical reaction, and when TEA was added to the acidified mixture, the chemical shift was restored proving that the reversibility between protonation and deprotonation. The nature of the response to acid-base stimuli is

demonstrated to be the result of reversible protonation and deprotonation reactions. Therefore, the mechanism of fluorescence extinction in solution and film by TFA and **TPPT**6 is mainly due to triazine ring ionisation.

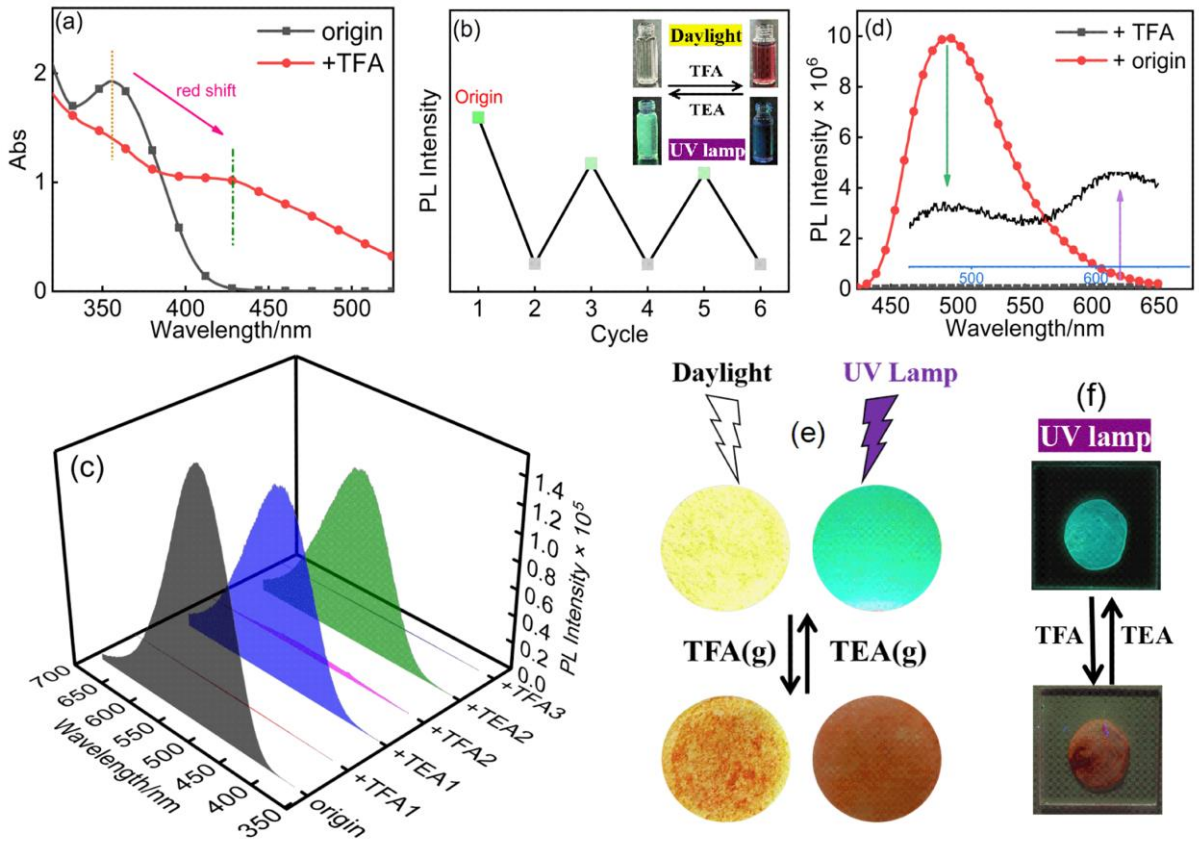

Figure 5. Photophysical properties of **TPPT**6 by acid-base (CF_3COOH/Et_3N) stimulation. UV-Vis absorption spectra (a); fluorescence periodic cycle diagram (b); emission spectra (c); solid sample fluorescence spectra before and after acid-base stimulation (d); sunlight/fluorescence images of solid samples (e); fluorescence images of thin films (f).

2.6 Mesomorphism

The mesomorphous behaviour of **TPPT**6/8/12 and **TPPT**6-H, a red solid compound formed by the fumigation of **TPPT**6 with trifluoroacetic acid, was investigated by polarized optical microscopy (POM) and differential scanning calorimetry (DSC), and the results are presented in Table 2, and Figures 6, S14 and S26 (see Supporting Information). **TPPT**12 and the ionic compounds exhibit optical dark fields caused by neatly aligned supramolecular columns orientated perpendicularly to the glass substrate, whereas the shorter-chain compounds exhibit focal conical texture. Differential scanning calorimetry show that **TPPT**6/8, **TPPT**6-H have only one heat endothermic peak during the second heating. The phase transition is identified by POM as the transition from a liquid crystal intermediate phase to isotropic liquid. **TPPT**12 undergoes two phase transitions, corresponding to solid-to-liquid crystal and liquid crystal-to-isotropic liquid, respectively. Comparison of **TPPT**6/8/12 reveals that the lengthening of the peripheral flexible chains leads to a significant decrease in the clearing point, and to the narrowing of the mesophase range.

Comparison of **TPPT**6 and **TPPT**6-H shows that **TPPT**6-H has a lower clearing point temperature of 43 °C and a more ordered stacking structure in POM, which is due to the formation of ionic bonds between the protonated triazine nitrogen atoms and the CF_3COO^- anion of TFA. The space-filling effect of the CF_3COO^- anion is responsible for the formation of a columnar phase of the "three-bladed propeller" molecule, which is more conducive to the orderly stacking of the molecules. This is also illustrated by the acid NMR titration of **TPPT**6. With the addition of TFA, the aryl hydrogens on the triphenylene unit show high-field displacement.

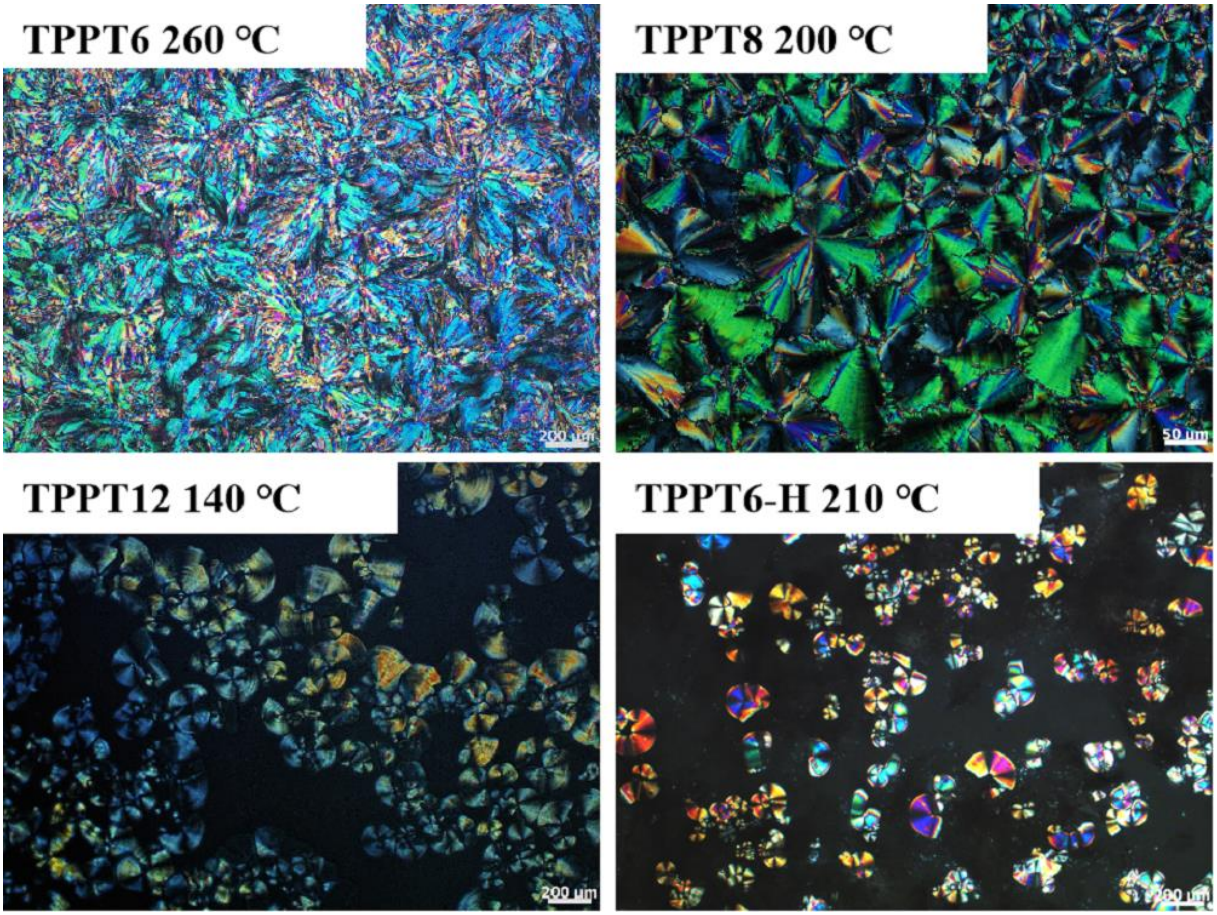

Figure 6. POM photo micrographs of **TPPT**6/8/12 and **TPPT**6-H.

Table 2. Phase transition temperatures and enthalpy changes of **TPPT**6/8/12 and **TPPT**6-H[a]

Compd.	2nd heating [1st cooling]/°C (*ΔH*/(kJ•mol^{-1}))[b]
TPPT6	Col_{rec} 278 (36.26) I [I 263 (38.85) Col_{rec}]
TPPT8	Col_{rec} 231 (27.90) I [I 221 (29.40) Col_{rec}]
TPPT12	Cr -7 Col_{rec} 149 (12.19) I [I 153 (14.94) Col_{rec} -13 Cr]
TPPT6-H	Col_{rec} 221 I [I 220 Col_{rec}]

[a] Col_{rec}: columnar rectangular mesophase; I, isotropic liquid; Cr: crystalline phase. [b] enthalpy change.

The liquid crystal phases of the target compounds were investigated by small-angle/wide-angle X-ray scattering (S/WAXS, Figures 7 and 8, and Table 3). After cooling from the isotropic liquid to the liquid crystal state, **TPPT**6/8/12 show broad and strong X-ray scattering peaks around 0.35-0.40 nm in the wide-angle region, which is

the characteristic scattering peak of π–π stacking of aromatic nuclei in supramolecular columns, and the wide and strong dispersion peaks around 0.43-0.45 nm, which are the characteristic scattering peaks of alkyl chains in the liquid molten state. The rigid nuclei of the liquid crystal molecules show orderly stacked supramolecular columns while the flexible chains are in the liquid state.

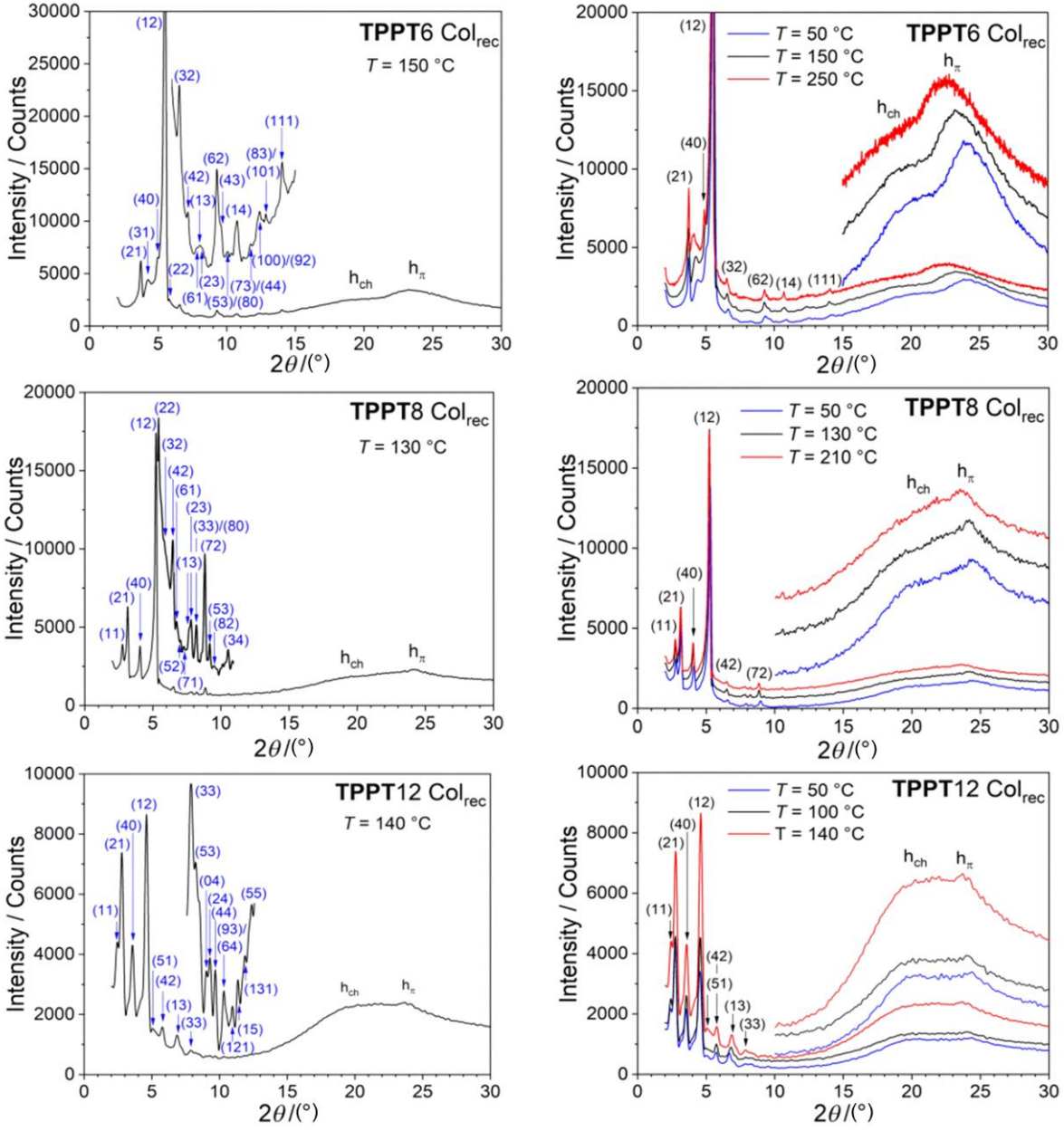

Figure 7. Representative SAXS/WAXS patterns of **TPPT***n* compounds at one temperature (left column) and with different temperatures (right column).

The structural analysis of the complex small-angle scattering patterns in combination with the geometrical size of the molecules suggest that the two-dimensional arrangement of the molecules in the liquid crystalline state is related to a supramolecular arrangement in a superlattice. The small-angle region of **TPPT**6 is dominated by two strong sharp peaks (2.35 nm, 1.59 nm) and two relatively weak scattering peaks (1.32 nm, 0.96 nm), which can be indexed according to Miller indices 21, 12, 32, 62, respectively, which are characteristic of a rectangular columnar phase. Measured and the theoretical values match perfectly. Similarly, in the small-angle

region of the X-ray patterns of **TPPT**8 and **TPPT**12, strong and sharp features characteristic rectangular columnar phases corresponding to Miller indices 21, 40, 12 can be found. The strong and sharp scattering peaks in the small-angle region, 2θ<5°, are attributed to the orderly stacking of the electron-rich rigid units of triphenylene and phenyltriazine in a rectangular superlattice too.

For **TPPT**6/8/12, the lattice parameters a and b gradually increase with the elongation of the alkoxy chains (a = 7.104～9.868 nm, b = 3.321～3.885 nm); the corresponding cell areas (A) were 23.5924, 30.2308, and 38.3372 nm^2. The results showed that **TPPT**6/8/12 self-assemble to form ordered rectangular columnar intermediate phase. Considering the molecular geometry and size of the "three-bladed propeller", as well as the X-ray diffraction profile and data, the proposed supramolecular model for the columnar rectangular phases is represented in Figure 8.

Table 3. Mesophase's parameters of the star-shaped triphenylene-triazine **TPPT***n*

TPPT6	TPPT8	TPPT12
Col_{rec}	Col_{rec}	Col_{rec}
a=7.104 nm, b=3.321 nm	a=8.692 nm, b=3.478 nm	a=9.868 nm, b=3.885 nm
A=23.5924 nm^2	A=30.2308 nm^2	A=38.3372 nm^2
V_{mol}=4.645 nm^3	V_{mol}=5.450 nm^3	V_{mol}=7.255 nm^3
h_{mol}=0.394 nm, N_{mol}=2	h_{mol}=0.360 nm, N_{mol}=2	h_{mol}=0.378 nm, N_{mol}=2

Lattice parameters: a, b; lattice area: A; molecular volume: V_{mol}; average molecular thickness, h_{mol}; number of molecules per lattice, N_{mol}, deduced from $N_{mol}.V_{mol} = A.h_{mol}$.

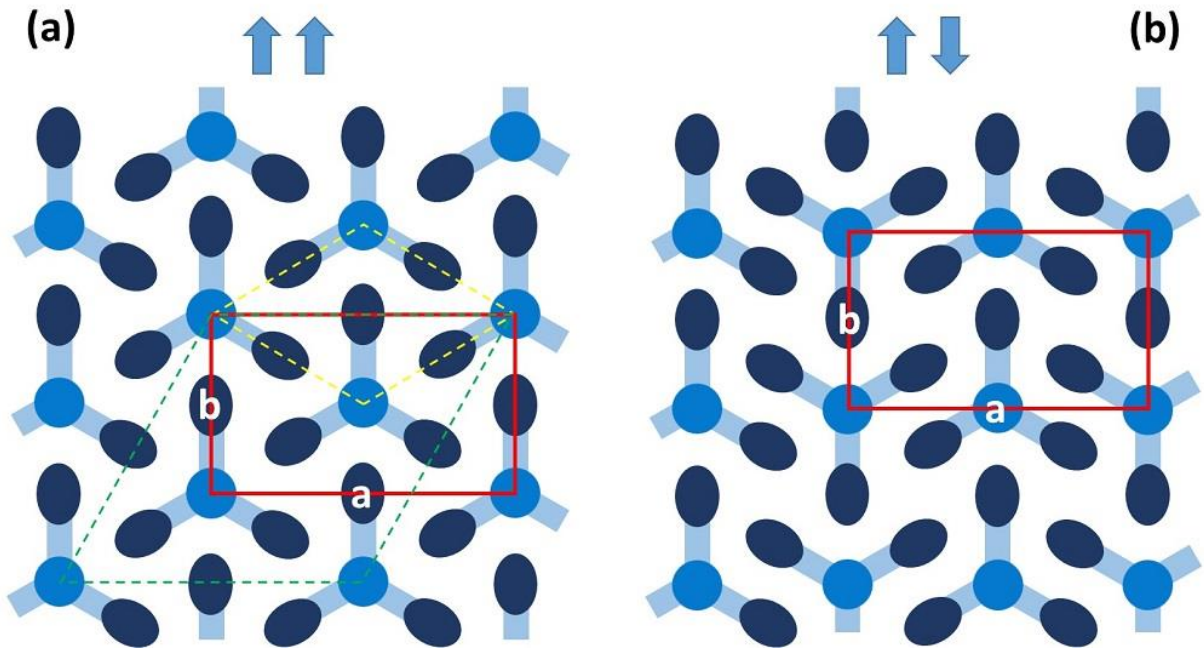

Figure 8. Two-dimensional supramolecular packing model of **TPPT***n* rectangular columnar liquid crystal phase (Col_{rec}), a rectangular superlattice containing two molecules. (a) parallel and (b) antiparallel arrangements of the trimers.

2.7 Applied Research

2.7.1 Safety Ink and Acid-Base Sensing

Security Information Technology (SIT) is an important technology for information processing. Based on the **TPPT**6 acid-base stimulus response, two security inks were designed (see Figure 9).

3 mg **TPPT**6 was dissolved in a 10 mL chloroform solution and diluted to 10^{-5} mol/L to obtain ink 1. "ZKX" was written on a filter paper with a skimmed cotton pad dipped in the ink, the writing disappeared after drying. The message was initially encrypted, and the green colour of the writing was clearly visible under UV light. The filter paper was then fumigated with trifluoroacetic acid (TFA) vapour, **TPPT**6 was protonated into **TPPT**6-H, and the red letters "ZKX" appear in daylight, and the message is decrypted. Then steam fumigate with triethylamine (TEA), **TPPT**6-H is deprotonated, and the red writing disappears, and the message encrypted again. Under UV light the letters are seen again (green fluorescence). Followed by alternating fumigation with TFA and TEA, repeated encryption and decryption of information is possible. TFA was added to ink 1 until the solution changes its colour to reddish-orange to yield ink 2, which was different from ink 1 in that it could write directly in red. Then, the information was repeatidly encrypted and decrypted by alternating fumigation with TEA and TFA vapour, respectively.

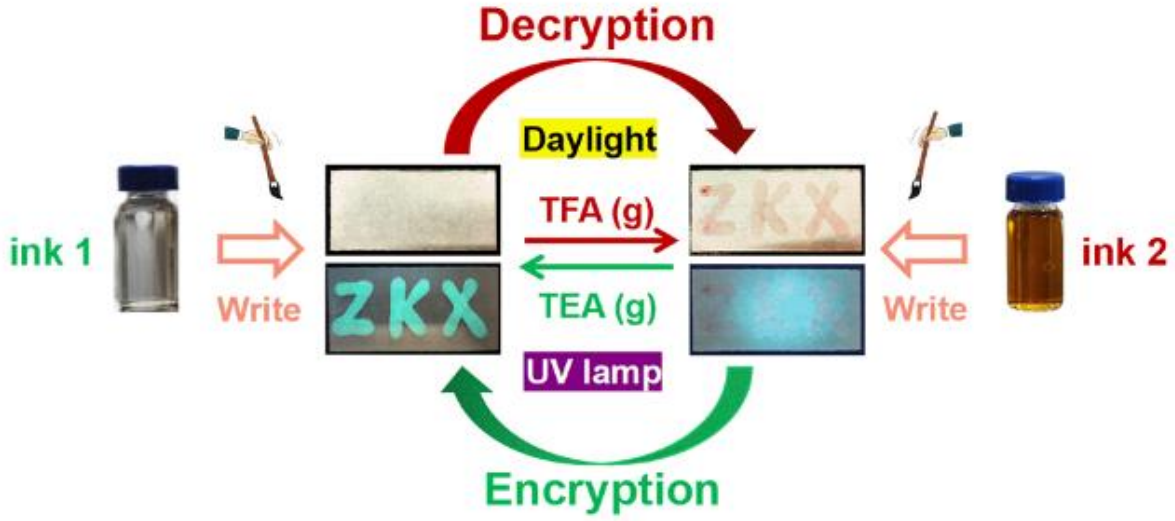

Figure 9. TPPT6 application as safety ink. Ink 1: diluted solution of **TPPT**6 in $CHCl_3$; Ink 2: ink 1 and CF_3COOH.

In addition, the fluorescence spectra of **TPPT**6 in chloroform solution with different levels of TFA (see Supporting Information, Figure S18) showed that the fluorescence was gradually extinguished with the increase of TFA gradient, and the fluorescence intensity changed in a good logarithmic relationship with the concentration of TFA (R2 = 0.987), which proved that **TPPT**6 has the potential application value in acid sensing and information encryption.

2.7.2 Electroluminescence and Organic Light-Emitting Diodes (OLEDs)

Based on the good luminescence properties of **TPPT**6 in the solid state and the better charge transfer semiconductor properties of discotic liquid crystals, we explored the electroluminescence (EL) performance and application in solid-state organic light-

emitting diodes (OLEDs). The device preparation was carried out according to the literature method [12,61]: Firstly, 5 g of silica gel was mixed with 20 mg of **TPPT**6 and then degassed in vacuum. The resulting mixture was cured with InGaN blue chips for 1 h to produce the OLED optics. The optical properties and chromaticity were measured and the results are shown in Figure 10 and Table S4 (see Supporting Information).

Through the electroluminescence optical spectrum of **TPPT**6, the OLED optics at 3.6 V turn-on voltage shows an emission peak at 502 nm. The OLED device shows good electroluminescence performance in a dark environment with a lime green light. Combined with CIE1931 colour chart, the colour coordinates of OLED x = 0.2493, y = 0.4622, present a greenish light, with a colour temperature Tc = 7838 K, which is a cool colour light (Tc > 5000).

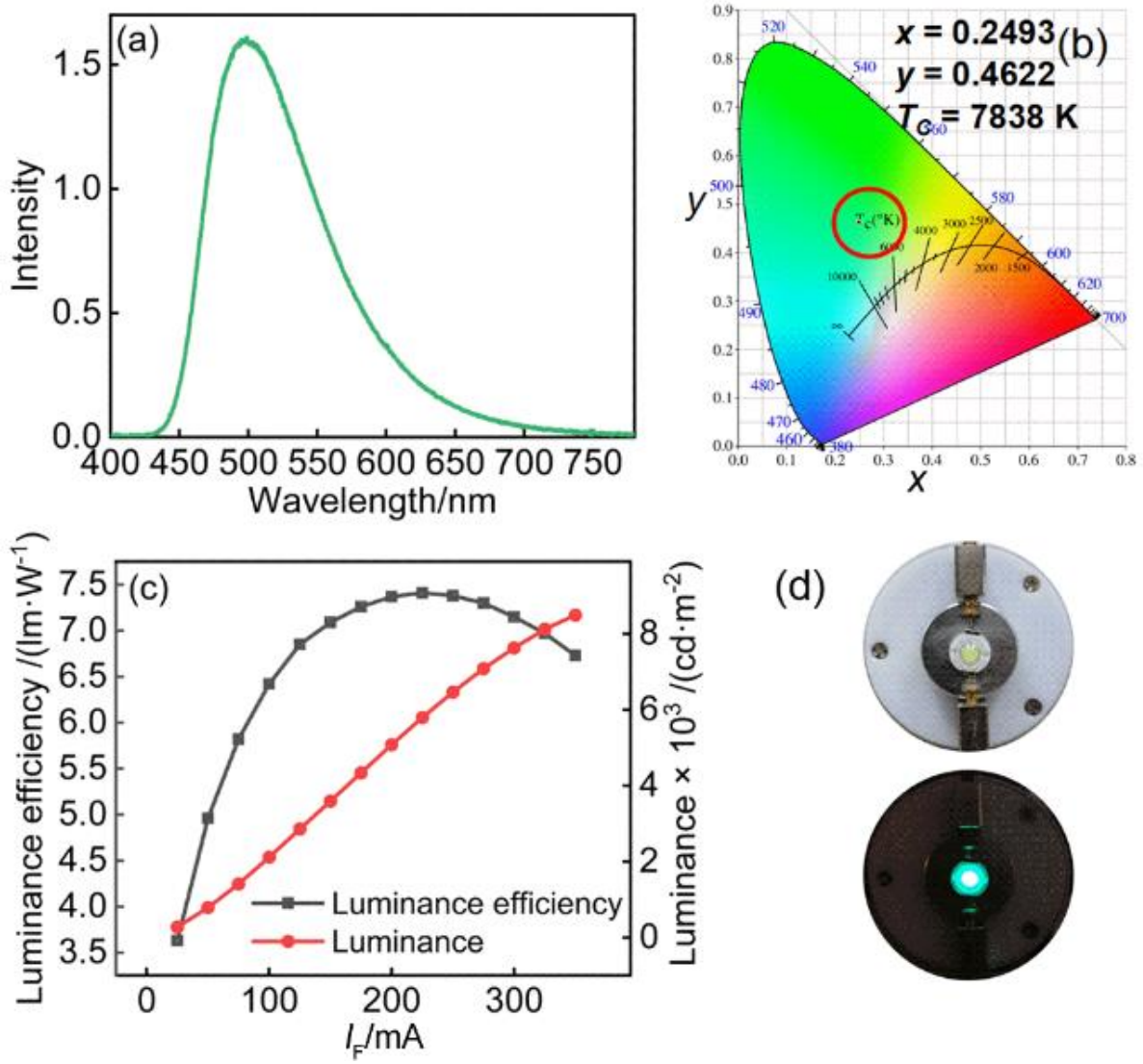

Figure 10. Electroluminescence spectra of **TPPT**6 (a), CIE 1931 chromaticity diagram (b), forward current versus luminous efficiency at constant voltage, light intensity relationship diagram (c), photos of OLED devices with and without electricity (d).

Varying the forward current at a constant voltage (3.6 V), the luminescence efficacy shows an inverted U-shaped curve in the forward current range of 25-350 mA, and reaches a maximum luminous efficacy of 7.41 lm/W at IF = 225 mA, which is nearly 35

times higher than that of the triphenylene-containing OLEDs reported by Kim et al. in 2013 [50] at the same current density/voltage and 3.5 times higher than that of the four triphenylene derivatives reported by Togashi et al. in 2012 [49], and than of the CTpCN OLEDs reported by Chantanop et al. [51] in 2022. The fluorescence efficiency is 1.59%, and does not change much under a wide current range from 175 to 275 mA, which indicates that the stability of the device is good in this range, which is favourable for potential application. The luminous efficacy (estimated by Φ=I-Sr, Sr is the sphericity, I is the luminosity) is also very good increasing linearly up to 8494 cd/m^2.

In addition, the colour rendering index of OLEDs does not change significantly with the change of forward current, indicating that the device has good chromaticity stability. Therefore, **TPPT**6 has a good potential for application as OLEDs, which provides a good opportunity for the design, synthesis and preparation of all-organic green OLEDs.

3 Conclusion

Star-type triazine-triphenylene-containing functional molecules **TPPT**6/8/12 for photovoltaic applications were synthesised by Suzuki-Miyaura coupling reaction and properly characterised. All the molecules show good aggregation-induced luminescence, effectively overcoming the disadvantage of aggregation-induced fluorescence quenching observed in most discotic molecules.

TPPT6 exhibits obvious solvation discolouration by intra-substrate charge transfer in the D-A structure, which is definitely the most important factor in the development of the D-A structure. **TPPT**6 shows significant solvatochromism affected by the intrafraction charge transfer of D-A structure, and the absolute quantum yield could reach up to 43%; **TPPT**6 shows thermochromism with fluorescence enhancement with temperature increase in organic solution; **TPPT**6 shows acidic discolouration by protonation with TFA. **TPPT**6 exhibits acidic discolouration; **TPPT**6/8/12 have wide rectangular columnar (Col_{rec}) liquid crystal intermediate phases, the widest of which reaches 278 °C. TFA can regulate the mesocrystalline behaviour through protonation/ionisation. **TPPT**6 has good electroluminescent properties and can be used for the preparation of OLEDs, with a maximum luminous efficacy of 7.41 lm/W. The triphenylene-triazine propeller compounds have potential applications in the fields of liquid crystal semiconductor materials, information encryption, and OLED light-emitting materials.

References

[1] Zhang J.; He B. Z.; Hu Y. B.; Alam P.; Zhang H. K.; Lam J. W. Y.; Tang B. Z. Adv. Mater. 2021, 33, 2008071.

[2] Yu X. W.; Zhang H. Y.; Yu J. H. Aggregate 2021, 2, 20.

[3] Han H. H.; Tian H.; Zhang Y.; Sedgwick A. C.; Li J.; Sessler J. L.; He X. P.; James T. D. Chem. Soc. Rev. 2021, 50, 9391.

[4] Feng Y. Q.; Wang N. N.; Ju H. X. Sci. China Chem. 2022, 65.

[5] Thomas D.; Rubio V.; Iragavarapu V.; Guzman E.; Pelletier O. B.; Alamgir S.; Zhang Q.; Stawikowski M. J. ACS Chem. Neurosci. 2021, 12, 719.

[6] William P. L.; Shen Z. Q.; Simon J. T.; Nasir J.; Ever V.; Deirdre M. C.; Li J. Chem. Sci. 2020, 11, 1814.

[7] Yang X.; Zhang Z. Y.; Su M.; Song Y. L. Acta Chimica Sinica 2022, 80, 80. (in Chinese). (杨旭, 张泽英, 苏萌, 宋延林, 化学学报 2022, 80, 80.)

[8] Jiang Y. Z.; Hu M. L.; Liu A. A.; Lin Y.; Liu L. L.; Yu B.; Pang D. W.; Zhou X. M. ACS Sens. 2021, 6, 1086.

[9] Fang W. Y.; Cao Z.; Liu Q. M.; Chu Y. H.; Zhu H. F.; Zhou W. W.; Yang J. X. RIO. 2022, 7, 100228.

[10] Weng Q. H.; Yi J. Q.; Chen X. P.; Luo D. W.; Wang Y. D.; Sun W. M.; Kang J.; Han Z. Z. ACS Omega. 2020, 5, 24864.

[11] Hariharan P. S.; Venkataramanan N. S.; Moon D.; Anthony S. P. J. Phys. Chem. C 2015, 119, 9460.

[12] Zeng C. Y.; Li D. H.; Cao Z.; He Y. R.; Gao Y. S.; Ye T. T.; Zhou W. W.; Fang W. Y. RIO. 2022, 8, 100264.

[13] Li Y. B.; Zhao. K. Q.; Yang Y. L.; Deng K.; Zeng Q. D.; Wang C. Nanoscale 2012, 4, 148.

[14] Jiang Y. H.; Wang Y. C.; Hua J. L.; Tang J.; Li B.; Qian S. X.; Tian H. Chem. Comm. 2010, 46, 4689.

[15] Meng P.; Han C. H.; Scully A. D.; Xiao Q.; Brock A. J.; Hirai T; Skidmore M.; McMurtrie J. C.; Chesman A. S. R.; Xu J. S. ACS Appl. Mater. Interfaces 2021, 13, 40441.

[16] Shahari M. S. B.; Dolzhenko A. V. Eur. J. Med. Chem. 2022, 241, 114654.

[17] Galindo J. M.; Leganes J.; Javier P.; Ana M. R.; Herrero M. A.; Enrique D. B.; Merino S.; Ana M. S.; Ester V. ACS Macro. Lett. 2019, 8, 1391.

[18] André A. V.; Giliandro F.; Wallison C. C.; Juliana E.; Ivan H. B.; Fabien D.; Harald B. Chem. Eur. J. 2021, 27, 9003.

[19] Lee C. J.; Lee S. J.; Chang J. Y. Tetrahedron Lett. 2002, 43, 3863.

[20] Lo W. J.; Hong Y. L.; Lin R. H.; Hong J. L. Mol. Cryst. Liq. Cryst. 2006, 308, 133.

[21] Lee C. H.; Yamamoto T. Bull. Chem. Soc. Jpn. 2002, 75, 615.

[22] Lee C. H.; Yamamoto T. Section A. Mol. Cryst. Liq. Cryst. 2002, 378, 13.

[23] Cristiano R.; Eccher J.; Ivan H. B.; Catarina N. T.; André A. V.; Molin F.; Gallardo H. Langmuir 2012, 28, 11590.

[24] Yasuda T.; Shimizu T.; Liu F.; Ungar G.; Kato T. J. Am. Chem. Soc. 2011, 133, 13437.

[25] Feringan B.; Romero P.; Serrano J. L.; Gimenez R.; Sierra T. Chem. Eur. J. 2015, 21, 8859.

[26] Taing H.; Jacob G. R.; Justin F. B.; Charles L. B. Liq. Cryst. 2018, 45, 1147.

[27] Cheng X. H.; Jin J.; Li Q.; Dong X. Chin. J. Chem. 2010, 28, 1957.

[28] Nihat A.; Mohammed H. A. A.; Belkız B. E.; Hale O.; Lokman T. Turk. J. Chem. 2019, 43, 1436.

[29] Beatriz F.; Roberto T.; Attilio G.; José M. G.; Amparo N.; Raquel G.; Teresa S. J. Mater. Chem. C 2021, 9, 1972.

[30] Kumar S. Liq. Cryst. 2004, 31, 1037.

[31] Zhao K. Q.; Wang B. Q.; Hu P.; Li Q.; Zhang L. F. Chin. J. Chem. 2005, 23, 767.

[32] Zhao K. Q.; Hu P.; Wang B. Q.; Yu W. H.; Chen H. M.; Wang X. L.; Shimizu Y. Chin. J. Chem. 2007, 25, 375.

[33] Wang C. L.; Dong H. L.; Hu W. P.; Liu Y. Q.; Zhu D. B. Chem. Rev. 2012, 112, 2208. [34] Zhao K. Q. J. Sichuan Normal University (Natural Science), 2019, 42, 286. (in Chinese). (赵可清. 四川师范 大学学报自然科学版. 2019, 42, 286.)

[35] Deng W. J.; Liu S.; Lin H.; Zhao K. X.; Bai X. Y.; Zhao K. Q.; Hu P.; Wang B. Q. New J. Chem. 2022, 46, 7936.

[36] Yang F. F.; Xie J. W.; Guo H. Y.; Xu B. T.; Li C. C. Liq. Cryst. 2012, 39, 1368.

[37] Umesh C. P.; Gangarapu S.; Marcelis A. T. M.; Zuilhof H. Liq. Cryst. 2014, 41, 1862.

[38] Bai Y. F.; Chen L. Q; Hu P.; Luo K. J.; Yu W. H.; Ni H. L.; Zhao K. Q.; Wang B. Q. Liq. Cryst. 2015, 42, 1591.

[39] Feng H. Y.; Geng X. T.; Lin J. R.; Guo H. Y.; Yang F. F. Liq. Cryst. 2018, 45, 1470.

[40] Hu R. R.; Leung N. L. C.; Tang B. Z. Chem. Soc. Rev. 2014, 43, 4494.

[41] Mei J.; Leung N. L. C.; Kwok T. K.; Lam W. Y.; Tang B. Z. Chem. Rev. 2015, 115, 11718.

[42] Yan Q.; Wang S. Mater. Chem. Front. 2020, 4, 3153.

[43] Yang J.; Chi Z. G.; Zhu W. H.; Tang B. Z.; Li Z. Sci. China Chem. 2019, 62, 1090.

[44] Yu W. H.; Chen C.; Hu P.; Wang B. Q.; Carl R.; Zhao K. Q. RSC Adv. 2013, 3, 14099.

[45] An B. K.; Kwon S. K.; Jung S. D.; Park S. Y. J. Am. Chem. Soc. 2002, 124, 14410.

[46] Voskuhl J.; Giese M. Aggregate 2022, 3, 124.

[47] Xia Z. G.; Liu Q. Lin. Prog. Mater. Sci. 2016, 84, 59.

[48] Seguy I.; Jolinat P.; Destruel P.; Farenc J.; Mamy R. J. Appl. Phys. 2001, 89, 5442.

[49] Togashi K.; Nomura S.; Yokoyama N.; Yasuda T.; Adachi C. J. Mater. Chem. C 2012, 22, 20689.

[50] Kim S. O.; Jang H. S.; Lee S. J.; Kim Y. K.; Yoon S. S. Bull. Chem. Soc. Jpn. 2013, 34, 2267.

[51] Chantanop N.; Nalaoh P.; Chasing P.; Wijitra W.; Sudyoadsuk T.; Promarak V. J. Lumin. 2022, 248, 118926.

[52] Bala I. D.; Yang W. Y.; Gupta S. P.; De J.; Kumar R. A. Y.; Singh D. P.; Dubey D. K.; Jou, J. H.; Doualid R.; Pal S. K. J. Mater. Chem. C 2019, 7, 5724.

[53] Lin H.; Zhao K. X; Jing M.; Long X. H.; Zhao K. Q.; Hu P.; Wang B. Q.; Lei P.; Zeng Q. D.; Donnio B. J. Mater. Chem. C 2022, 10, 14453.

[54] (a) Zhao K. C.; Zhao K. Q.; Hu P.; et al. Chem. Asian J. 2019, 14, 462. (b) Liu C. X.; Du J. Q.; Zhao K. Q.; et al. J. Mater. Chem. C 2018, 6, 4471. (c) Ma T.; Zhao K. Q.; Wang B. Q.; et al. ChemPlusChem. 2019, 84, 1439. (d) Zhong Y. J.; Zhao K. Q.;

Heinrich B. Dyes Pigm. 2020, 173, 107964. (e) Ma Tao, Zhao K. Q.; Monobe H.; et al. Chem. Asian J. 2021, 16, 1106.

[55] Zhang L. L.; Wang Y. Y.; Zhu G. N.; Dai W. B.; Zhao Z. X.; Zhao Y.; Zhi J. G.; Dong Y. P. Acta Chimica Sinica 2022, 80, 282. (in Chinese). (张璐璐, 王媛媛, 朱贵楠, 戴文博, 赵紫璇, 赵盈, 支俊格, 董宇平, 化 学学报, 2022, 80, 282.)

[56] Liu T. H.; Yang L. J.; Liu K.; Ran Q.; Feng W.; Wang W. N.; Liu Q.; Peng H. N.; Ding L. P.; Fang Y. ACS Appl. Mater. Interfaces 2020, 12, 11084.

[57] Huang R. R; Liu H. J.; Liu K.; Wang G.; Liu Q.; Wang Z. L.; Liu T. H.; Miao R.; Peng H. N.; Fang Y. Anal. Chem. 2019, 91, 14451.

[58] Hong Y. N.; Tang B. Z.; Lam J. W. Y. Chem. Comm. 2009, 6, 4332.

[59] Hong Y. N.; Tang B. Z.; Lam J. W. Y. Chem. Soc. Rev. 2011, 40, 5361.

[60] Zhang J.; Li A. S.; Zou H.; Peng J. H.; Guo J. L.; Wu W. J.; Zhang H. K.; Zhang J.; Gu X. G.; Xu W. Q.; Xu S. P.; Liu S. H.; Qin A. J.; Lama J. W. Y.; Tang B. Z. Mater. Horizons. 2020, 7, 135.

[61] Fang W. Y.; Zhao W.; Pei P.; Liu R.; Zhang Y. Y.; Kong L.; Yang J. X. J. Mater. Chem. C 2018, 6, 9269.